石 油 学 报

(石油加工)

第 34 卷 第 6 期 2018 年 11 月(卷终)

目 次

* 封面文章

期刊基本参数:CN11-2129/TE * 1985 * b * A4 * 198 * zh+en * P * ¥20.00 * 1200 * 27 * 2018-11 **本期责任编辑**:杨华英

ACTA PETROLEI SINICA

(PETROLEUM PROCESSING SECTION)

Vol .34 No .6 Nov. 2018

CONTENTS

Research Articles

Acta Petrolei Sinica (*Petroleum Processing Section*), 2018, 34(6): 1075-1081 **doi**: 10.3969/j.issn.1001-8719.2018.06.003

Catalytic Oxidation of Furfural to Maleic Acid by Hierarchical Molecular Sieves CoAPO-5 in Aqueous Phase

LU Yang LI Qiao WANG Jun SUN Xueni SHAO Hui HUANG Chunxiang ZHONG Jing

Compared with the microporous molecular sieves CoAPO-5, the hierarchical molecular sieves CoAPO-5 have larger pore size and more acidity .In the catalytic reaction of furfural to Maleic acid in aqueous phase, the hierarchical molecular sieves CoAPO-5 show better catalytic efficiency .

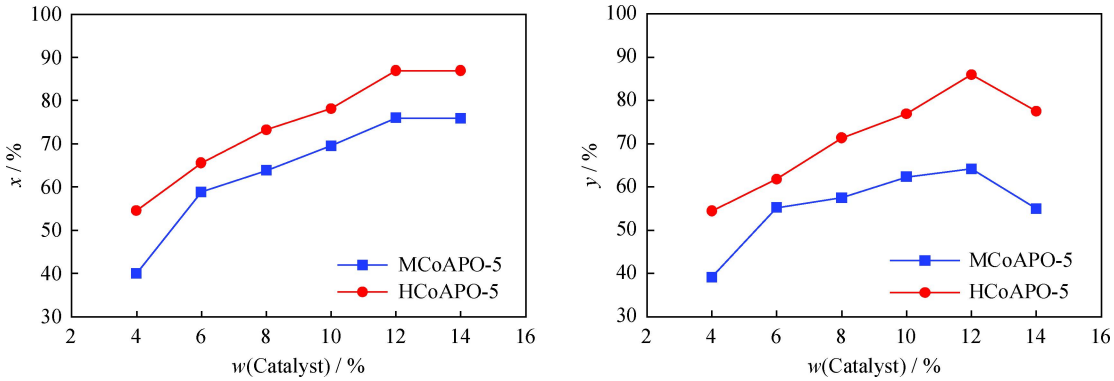

Acta Petrolei Sinica (*Petroleum Processing Section*), 2018, 34(6): 1082-1088 **doi**: 10.3969/j.issn.1001-8719.2018.06.004

Reaction Performance and Mechanism for Decomposition of 2,4-Toluene Dicarbamate

WANG Guirong CUI Xuexia JIA Xiaoqiang ZHAO Xinqiang WANG Yanji

The TGA curves of dimethyl toluene-2,4-dicarbamate (TDC(Me)), dipropyl toluene-2,4-dicarbamate (TDC(Pr)), dibutyl toluene-2,4-dicarbamate(TDC(Bu)), and diphenyl toluene-2,4-dicarbamate (TDC(Ph)) are shown in the following figure. The thermal decomposition temperatures of toluene-2,4-carbamates imply the difficulty degree of decomposition reactions .

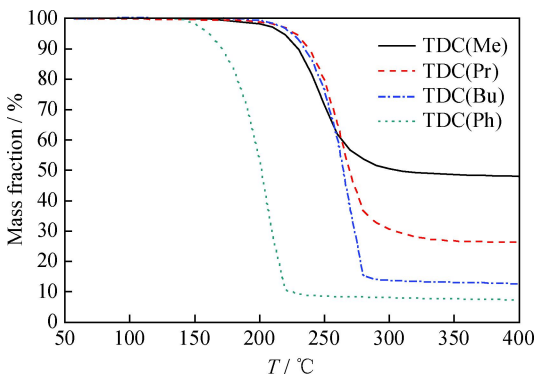

Acta Petrolei Sinica (*Petroleum Processing Section*), 2018, 34(6): 1089-1096 **doi**: 10.3969/j.issn.1001-8719.2018.06.005

Effects of Solvent for Copper and Zinc Nitrate on the Catalytic Performance of CuZnAl Catalyst Prepared by Complete Liquid-Phase Method

HUANG Li YANG Xiangfeng REN Hongwei FAN Jinchuan HUANG Wei

H_2-TPR profiles of catalysts prepared from different solvents were shown in the figure. The peak temperature of the CuZnAl catalyst prepared from ethylene glycol as the solvent was relatively higher than that prepared from water and ethanol as the solvent, indicating that the stronger interaction between the reducible Cu species and the Zn and Al species. All peaks are ascribed to the reduction of $Cu^+ \rightarrow Cu^0$, where the small peaks at low temperature are attributed to the reduction peak of the highly-dispersed Cu_2O interacting with ZnO. The high temperature reduction peaks are attributed to the highly-reduced Cu_2O interacting with the Al component.

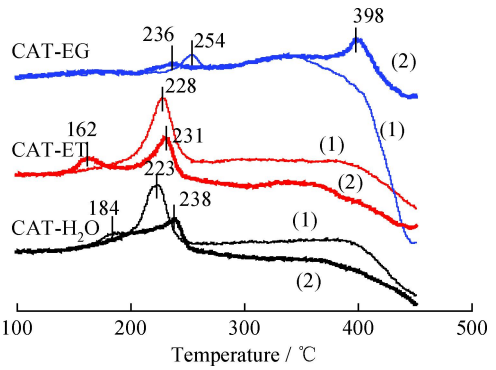

(1) Before reaction; (2) After reaction

Acta Petrolei Sinica (*Petroleum Processing Section*), 2018, 34(6): 1097-1103 **doi**: 10.3969/j.issn.1001-8719.2018.06.006

Synthesis, Characterization of Mesoporous TS-1 Zeolite and Its Catalytic Performance for Palmitic Acid Hydrodeoxygenation

ZHU Chaojie FU Wenqian ZHANG Lei TANG Tiandi

The hydrogenation reaction of palmitic acid was carried out by using mesoporous TS-1 zeolite supported metal nickel as catalyst. Through optimizing the reaction conditions, the highest catalyst activity and target products selectivity were obtained.

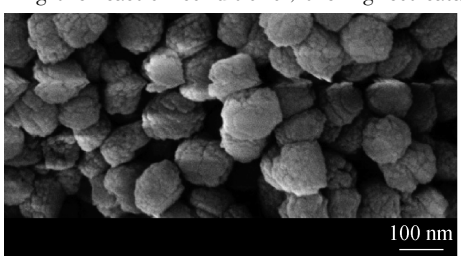

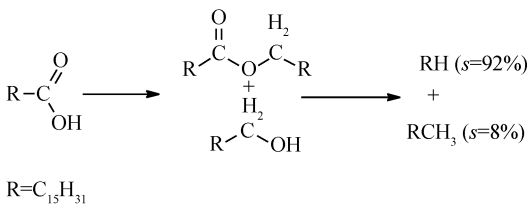

m(Ni/TS-1-M)=0.5 g, T=260℃, p_{H_2}=4 MPa, Stirring speed=300 r/min

Acta Petrolei Sinica (*Petroleum Processing Section*), 2018, 34(6): 1104-1110 **doi**: 10.3969/j.issn.1001-8719.2018.06.007

Effect of Feed Properties on the Hydro-Upgrading Reaction of Diesel Under Medium-Pressure Conditions

XU Xiaoling WANG Hua WEI Jun TIAN Lingyan

The saturation rate of aromatics at different reaction temperatures with feed A1, A2, B1 and B2 (the aromatic content of the feed decrease in the following order: A1>A2>B1>B2) is investigated.

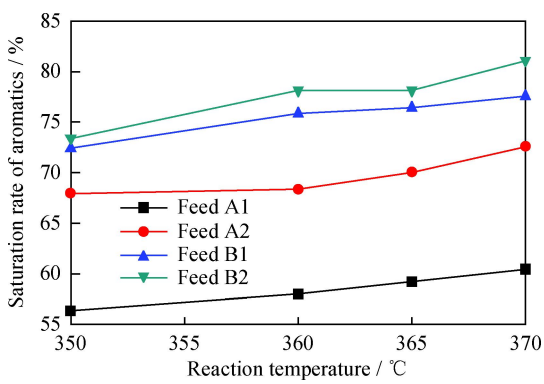

Acta Petrolei Sinica (*Petroleum Processing Section*), 2018, 34(6): 1111-1116 **doi**: 10.3969/j.issn.1001-8719.2018.06.008

Construction and Interfacial Effect of 2D/2D g-C_3N_4-rGO Composites

HAN Jianpeng WANG Shuaijun ZHAO Zhaocheng
LIU Zongmei WANG Yongjian ZHOU Anna

The correlation between interfacial and catalytic properties of CN-RGO interfacial composites was studied. Results show that the interfacial effect of CN-RGO interfacial composite obviously promotes the photocatalytic activity of CN-RGO interfacial composites, with the maximum degradation rate of 85.8%. The role of h^+ and O_2^-· in RhB photodegradation is more important than that of ·OH and H_2O_2.

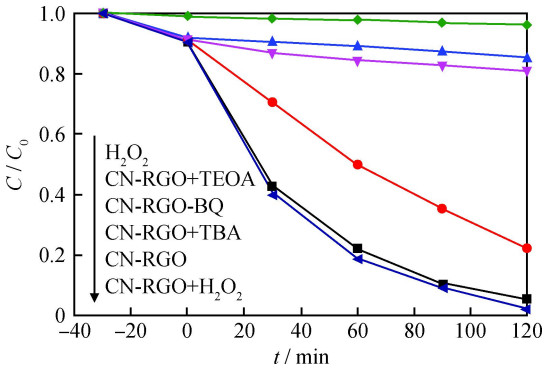

Acta Petrolei Sinica (*Petroleum Processing Section*), 2018, 34(6): 1117-1126 **doi**: 10.3969/j.issn.1001-8719.2018.06.009

Radial Distribution of Solid Holdup and Particle Velocity in Countercurrent-Variable Diameter Feedstock Injection Zone of an FCC Riser

BIAN Jing ZHAO Fengjing FAN Yiping LU Chunxi

On the basic of previous feedstock injection zone of an FCC (fluid catalytic cracking) riser, where the feed jets contacted counter-currently with particle flow from riser bottom, some improvement was made by changing the size of diameter, thus the countercurrent-variable diameter structure was brought up.

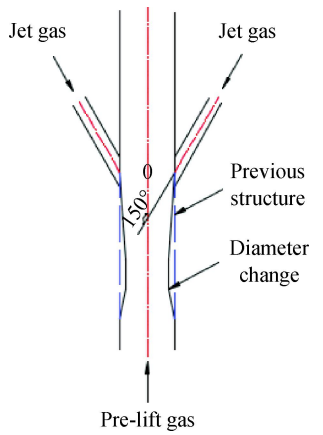

Schematic diagram of feed injection zone

Acta Petrolei Sinica (*Petroleum Processing Section*), 2018, 34(6): 1127-1135 **doi**: 10.3969/j.issn.1001-8719.2018.06.010

Prediction of H_2S Concentration in the Start-Up Pipeline of Delayed Coking Unit Based on Optimized RVFLN

XU Linfengyi OU Guofu JIN Haozhe

The cause of corrosion in the start-up pipeline of a delayed coking unit was analyzed, and data-driven model was developed to predict H_2S concentration in the start-up pipeline based on small norm random vector network.

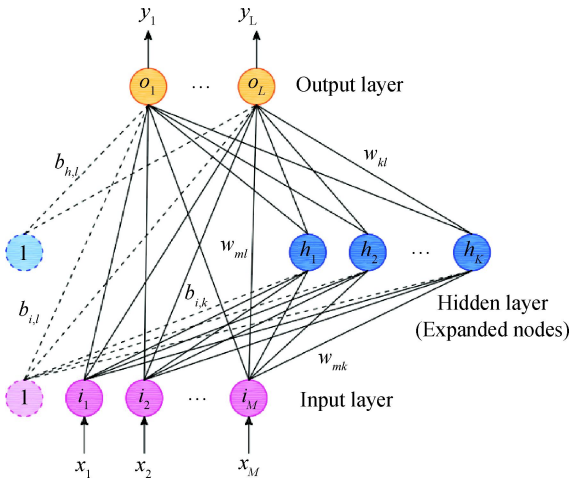

x—Inputs; y—Outputs; i_M—Value of M-th input node; h_K—Value of M-th expanded node; o_L—Value of L-th output node; $b_{i,k}$—Bias form input layer to the k-th expanded node; $b_{i,l}$—Bias form input layer to the l-th output node; $b_{h,l}$—Bias form hidden layer to the l-th output node; w_{mk}—Weight between the m-th input node and the k-th expanded node; w_{ml}—Weight between the m-th input node and the l-th output node; w_{kl}—Weight between the k-th expanded node and the l-th output node

Acta Petrolei Sinica (*Petroleum Processing Section*), 2018, 34(6): 1143-1148 **doi**: 10.3969/j.issn.1001-8719.2018.06.011

Size Distribution and Micro-Structure of PODE-Diesel Blended Fuel Combustion Particles

YANG Chen LIU Junheng SUN Ping JI Qian YAO Xiaohua

In this research, 10%, 20% and 30% (by volume) PODE were separately blended with diesel fuel. The experimental results show that, at maximum torque speed of 100% load, as the blending ratio increases, the number concentration distribution, mass density distribution, mass cumulative distribution and mass median diameter of combustion particles are all shifted to the small size direction. The particles fringe separation distance and fringe tortuosity of blended fuel increase while fringe length decreases.

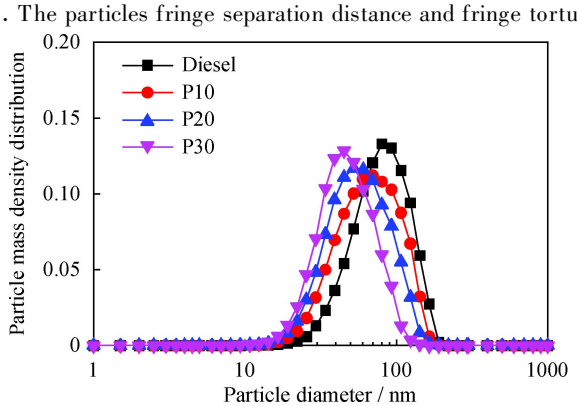

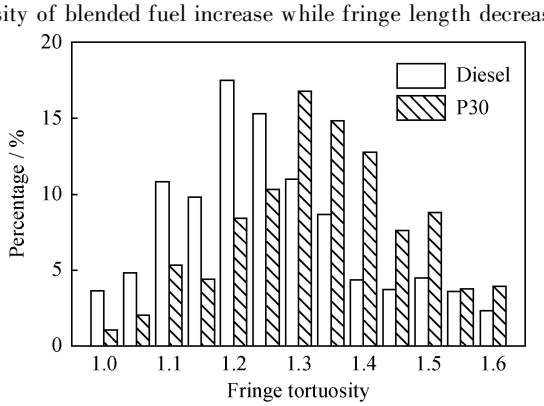

Acta Petrolei Sinica (*Petroleum Processing Section*), 2018, 34(6): 1143-1148 **doi**: 10.3969/j.issn.1001-8719.2018.06.012

Effect of Clarifying Agent Types on the Interfacial Stability of Different Crude Oil Components

WANG Manlin FANG Shenwen WANG Fei WANG Xiujun ZHAI Lei DUAN Ming

Three kinds of clarifying agents (cationic, amphoteric ionic, non-ionic) were studied. Simulating the residual polymers solutions, coalescence method was used to research the effects of the clarifying agents on interfacial stability of various component of crude oil considering different conditions of temperature and dosage, reasons were analyzed briefly combining with the result of interfacial tension. The experimental results demonstrated that the cationic clarifying agent interact with the asphaltene primarily and accelerating the coalescence process, the amphoteric ionic clarifying agent mainly react with the resin and asphaltene, and the non-ionic clarifying agent can interact with any component of the crude oil and facilitating the process.

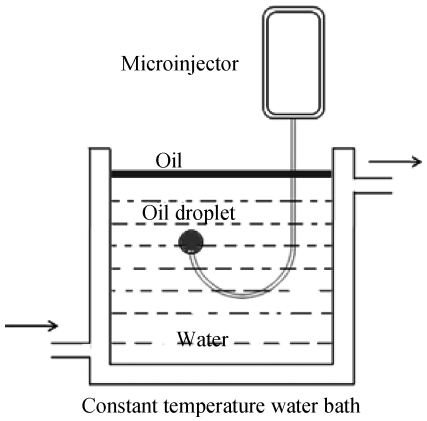

Acta Petrolei Sinica (*Petroleum Processing Section*), 2018, 34(6): 1149-1154 **doi**: 10.3969/j.issn.1001-8719.2018.06.013

Structure and Composition Characterization of Asphaltenes by Solid-Sate ^{13}C-NMR

SUN Yudong SONG Lifei HAN Zhongxiang WANG Yaochen TAO Yi

The structure model and parameters of asphaltenes were studied by solid-state ^{13}C-NMR. Experimental and calculation results indicate that asphaltene molecules consist of about 4 structural units, each containing 5 to 7 ploy-aromatic rings. For saturated carbons in asphaltenes, there are mainly naphthenic carbons with a few short alkyl side chains. The above result is different with that obtained by ^{1}H-NMR.

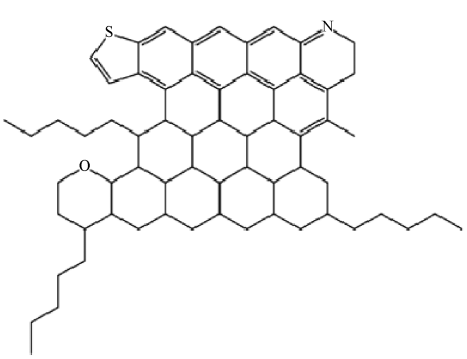

SL asphaltene

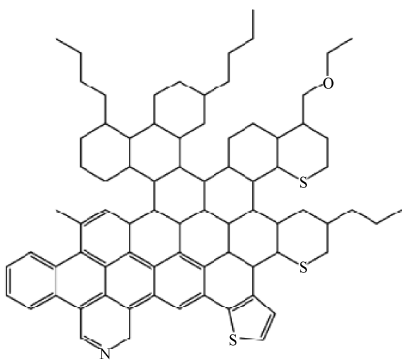

JD asphaltene

Acta Petrolei Sinica (*Petroleum Processing Section*), 2018, 34(6): 1155-1162 **doi**: 10.3969/j.issn.1001-8719.2018.06.014

Effects of Introduction Methods of Cerium Cations on Its Location in Y Zeolites

QIU Limei ZHENG Jinyu LU Lijun XIN Mudi XU Guangtong

The location of cerium cations in Y zeolites, which are introduced via ion-exchange method and one-step deposition method, was studied based on comprehensive routine practical characterization analysis, including XPS, XRD and Py-IR methods.

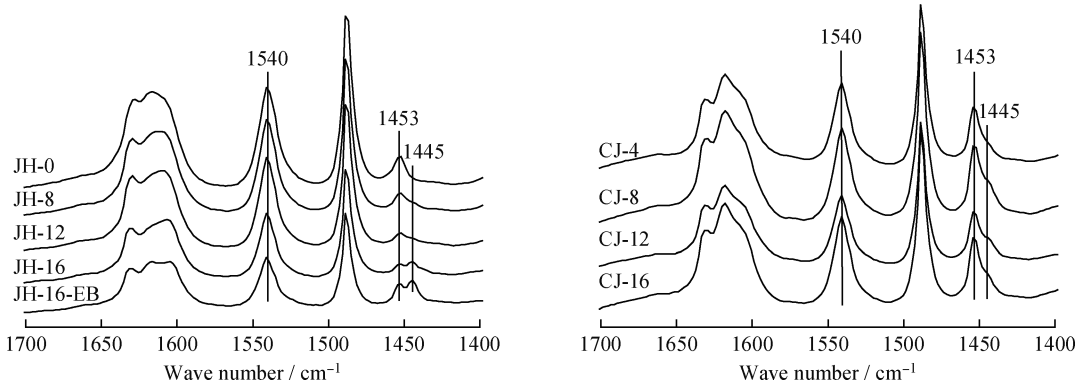

Research Notes

Acta Petrolei Sinica (*Petroleum Processing Section*), 2018, 34(6): 1163-1171 **doi**: 10.3969/j.issn.1001-8719.2018.06.015

Application Performance of Ceramic Membrane on Purifying FCC Slurry Oil

ZHANG Qiang ZHANG Zhiwei WANG Xin ZHANG Fuping
TANG Quanhong YANG Zhanxu WANG Dehui

The 50 nm ceramic membrane was used in the process of the purification treatment of FCC slurry oil. As indicated in the figure, the ceramic membrane can be divided into three sections, i.e. separating layer (the thinnest one, determining the filter precision), transition layer (the middle layer, linking separation layer and supporting layer) and the supporting layer(the thickness one, supporting the whole structure). This structure can prevent the ceramic membrane from contamination, and make it easy for regeneration.

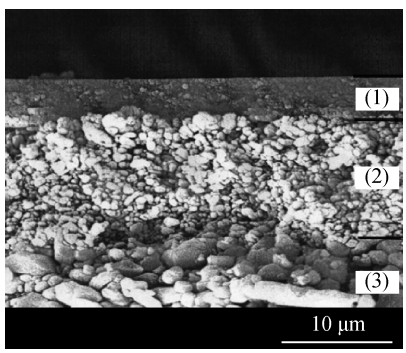

(1) Separating layer; (2) Transition layer; (3) Supporting layer

Acta Petrolei Sinica (*Petroleum Processing Section*), 2018, 34(6): 1172-1180 **doi**: 10.3969/j.issn.1001-8719.2018.06.016

Vortex Analysis for Cyclone Separators With Different Vortex Finder Diameters Based on *Q* Criterion

GAO Zhuwei WANG Juan WANG Jiangyun MAO Yu LI Jun WEI Yaodong

The changing trend of vortex structure can be visually observed based on the 3D iso-vortex surface extraction according to *Q* criterion. The vortex core oscillation does not increase linearly with vortex finder diameter, but has an optimum value. At the optimum point, the total vortex core oscillation can be minimized.

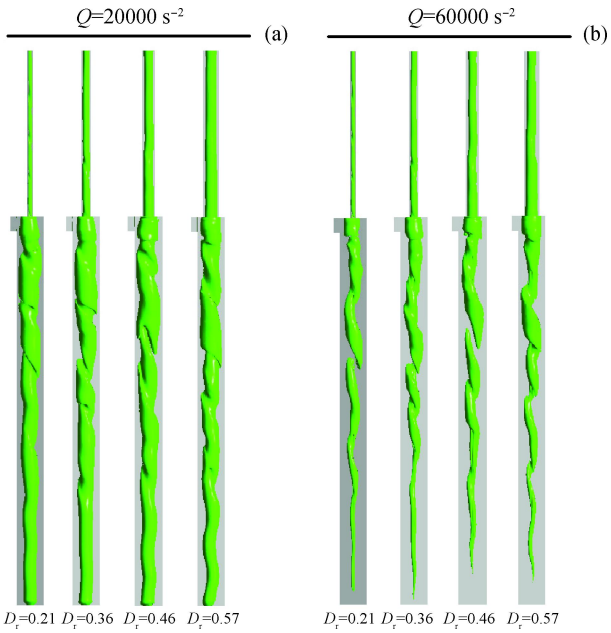

Acta Petrolei Sinica (*Petroleum Processing Section*), 2018, 34(6): 1181-1186 **doi**: 10.3969/j.issn.1001-8719.2018.06.017

Optimization of Experimental Conditions for Measurement of Toluene Insolubles in Heavy Oils by Response Surface Method

GAO Lei CHEN Lihan ZHAO Lixin DU Wei SHI Xin
GAO Yanan CHEN Gang JI Pengjun

Determination of toluene insolubles in heavy oils by the filtration method was discussed in the paper. Residues from crude oil were used in the study. On the basis of single-factor test, the response surface methodology was utilized to investigate the effects of toluene volume, temperature and filter size of filter membrane. The toluene insoluble mass fraction was chosen as response value. The following is a schematic diagram of vacuum glass filtration assembly.

Schematic diagram of vacuum glass filtration assembly

Acta Petrolei Sinica (*Petroleum Processing Section*), 2018, 34(6): 1187-1194 **doi**: 10.3969/j.issn.1001-8719.2018.06.018

Composition and Property Analysis of Solid Residues Extracted From Co-Hydrocracking Products of Coal and Atmospheric Residues

QIN Yong YANG Tengfei LI Chuan DENG Wenan

With lignite coal and Venezuela atmospheric residues as feedstocks, coal/oil co-hydrocracking was performed within an autoclave. Solid residues (toluene insolubles) were extracted from the above products and characterized with different techniques.

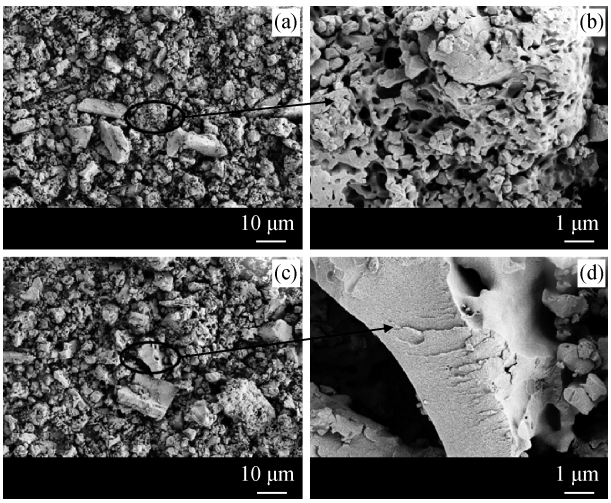

(a), (c) 1000× significance; (b), (d) 10000× significance

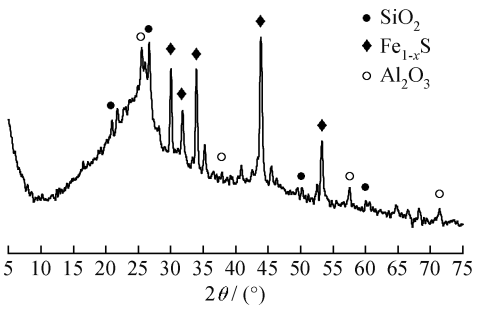

Acta Petrolei Sinica (*Petroleum Processing Section*), 2018, 34(6): 1195-1202 **doi**: 10.3969/j.issn.1001-8719.2018.06.019

Analysis on Factors Affecting Withdrawal Loss of Oil Floating Roof Tanks in Petrochemical Industry

WANG Yongqiang LIU Minmin LIU Fang CHEN Xi
WU Pengwei JIANG Shan

A model instrument of simulating the oil loading process by the stainless steel and carbon steel as the test piece was designed, and the film thickness is measured by wet film thickness gauge to investigate the effect of the tank wall corrosion and rim seal on the withdrawal loss for floating roof tanks.

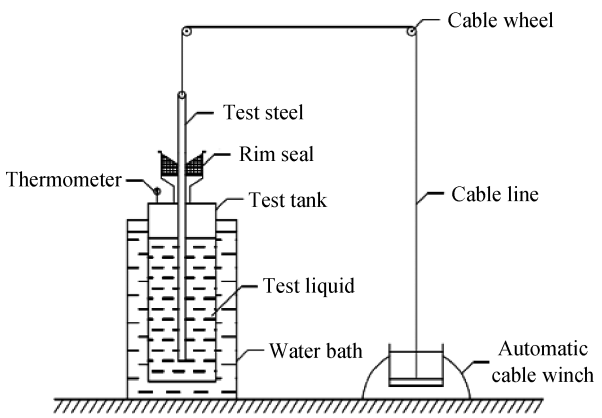

Acta Petrolei Sinica (*Petroleum Processing Section*), 2018, 34(6): 1203-1210 **doi**: 10.3969/j.issn.1001-8719.2018.06.020

Bioremediation of Petroleum Contaminated Soil by Wheat Straw and Microorganism

SHANG Qiongqiong ZHANG Xiuxia LI Zhenwei MA Nian LIU Zeyang LIU Huie

The wheat straw and bacteria mixture of *Alcaligenes* sp. J-1 and *Arthrobacter* sp. J-2 were used to study the bioremediation of petroleum-contaminated soil and the synergistic effect in the process. The correlation between petroleum hydrocarbon degradation rate and humic acid content was significant, with a correlation coefficient of 0.906. IMM had a better effect on remediation of soil.

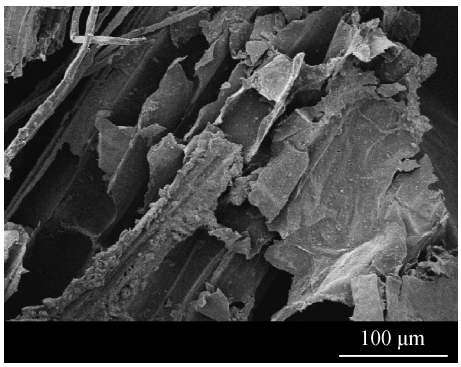

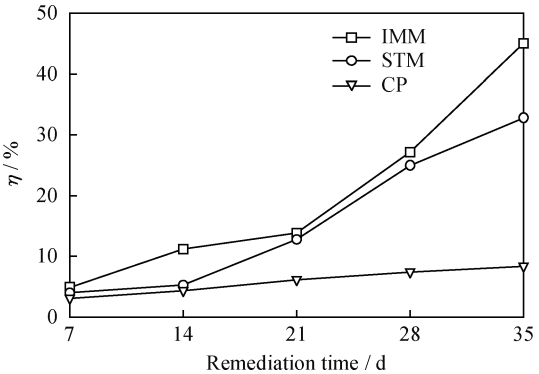

The 19th Chinese Zeolite Conference Articles

Acta Petrolei Sinica (*Petroleum Processing Section*), 2018, 34(6): 1211-1216 **doi**: 10.3969/j.issn.1001-8719.2018.06.021

Effects of Phosphorus Modification on the Stability of β Zeolite With and Without Template Removal

WANG Chengqiang OUYANG Ying LUO Yibin

After removing organic template agent, β zeolite was modified by phosphorus. The steric hindrance in zeolite crystal is reduced, with the increasing of accessibility between phosphorus species and the tetrahedral framework aluminum. Therefore, phosphorus can be efficiently coordinated with the tetrahedral framework aluminum, which inhibits the dealumination of molecular sieve framework. Consequently, β zeolite displays greatly improved structural stability under hydrothermal conditions.

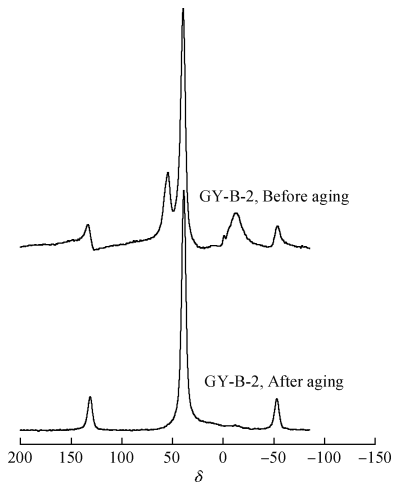

Acta Petrolei Sinica (*Petroleum Processing Section*), 2018, 34(6): 1217-1223 **doi**: 10.3969/j.issn.1001-8719.2018.06.022

Production of β Zeolite at Large Scale and Its Application in the Liquid Phase Alkylation of Benzene With Ethylene in Industrial Side-Line Experiment

CUI Long LI Jing ZHAO Yin LÜ Jianhui LI Zheng LI Wei
QIU Baojun LIANG Zuodong

100 kg β zeolite was synthesized in the 1 m^3 high pressure reactor. The self-made β zeolite was compared with the imported β zeolite. The catalytic evaluation of self-made β zeolite catalyst in liquid phase alkylation of benzene with ethylene reaction was carried out on industrial side-line equipment for 6072 h. And the impacts of the different mole ratio of benzene to ethylene, feed way, and temperature on the catalytic performance of self-made β zeolite catalysts were investigated. Results show that the catalyst meets the requirement of industrial production.

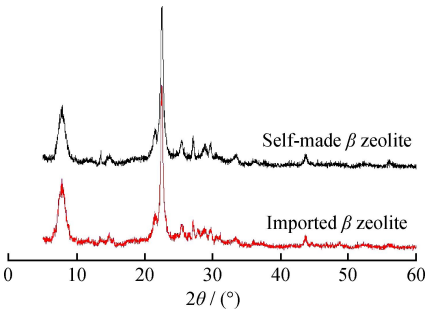

Acta Petrolei Sinica (*Petroleum Processing Section*), 2018, 34(6): 1224-1228 **doi**: 10.3969/j.issn.1001-8719.2018.06.023

Effect of Reaction Pressure on the Performance of Catalyst in *n*-Butene Isomerization Reaction

JIA Zhiguang REN Xingtao WU Kai YANG Guang

Bimolecular pathway and unimolecular pathway are two major mechanisms in *n*-butene isomerization, which mainly generate C_{5+} and isobutene respectively. In the later stage of the reaction, the unimolecular mechanism is the major dominant. The yield of isobutene increases by 2—3 percentage when the pressure changes from atmosphere to 0.05 MPa.

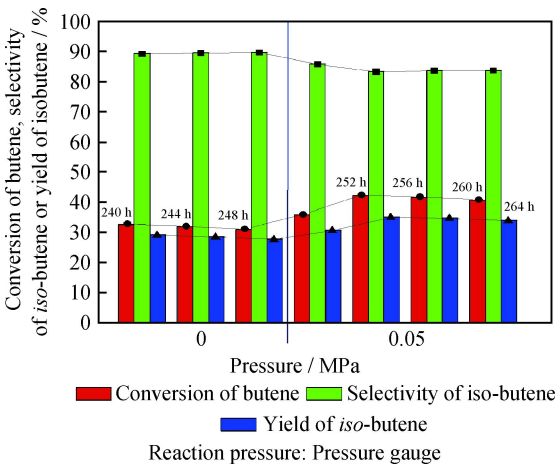

Acta Petrolei Sinica (*Petroleum Processing Section*), 2018, 34(6): 1229-1232 **doi**: 10.3969/j.issn.1001-8719.2018.06.024

Fabrication of Hierarchically Porous Structure of Strontium Titanate Photocatalyst

LI Wenxiu ZHANG Xiao JIA Aizhong WANG Yanji

Hierarchical pores were successfully fabricated in the Ni,La-$SrTiO_3$ with hard template prepared by coprecipitation method. The as-synthesized sample possesses large surface area of 180 m^2/g and hierarchical pore distribution, including micropores, mesopores and macropore, especially for supermacropore.

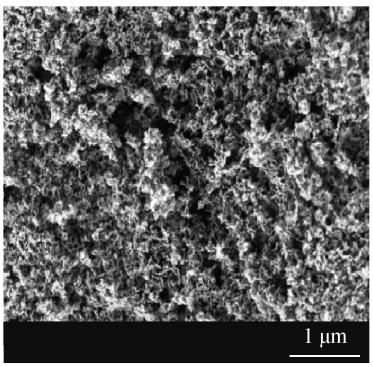

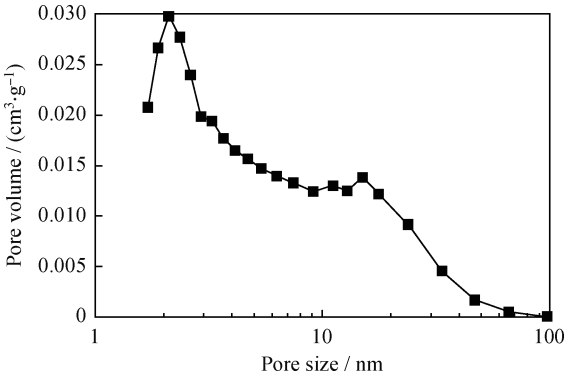

Acta Petrolei Sinica (*Petroleum Processing Section*), 2018, 34(6): 1233-1239 **doi**: 10.3969/j.issn.1001-8719.2018.06.025

Gas Alkylation of Ethanol With Benzene Over ZSM-11 Zeolite Catalysts Synthesized via Different Preparation Methods

XIN Wenjie ZHANG Shuang YANG Chuanyu LIU Shenglin
XU Longya

Among the Cat-A, Cat-B, Cat-C zeolite catalysts of similar strong acidity, Cat-A exhibits the highest benzene conversion in the gas alkylation reaction of ethanol with benzene, in the case of ethanol conversion less than 100%, under the same reaction conditions.

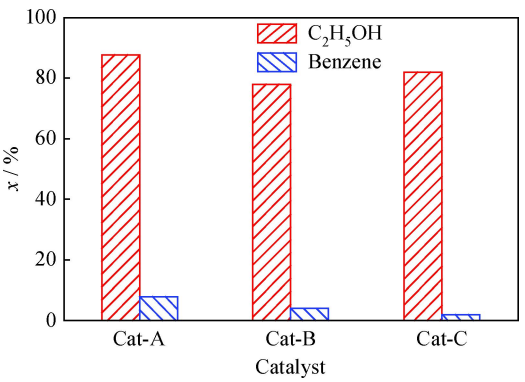

Acta Petrolei Sinica (*Petroleum Processing Section*), 2018, 34(6): 1240-1246 **doi**: 10.3969/j.issn.1001-8719.2018.06.026

Adsorption of Cu(Ⅱ) by ZSM-5 Zeolite Containing Organic Template in Aqueous Solution

ZHANG Shoulei LÜ Tianming FENG Zhe WANG Yu MENG Changgong

ZSM-5 zeolite containing HMD shows good ability in the adsorption of Cu^{2+} from aqueous solution. The maximum adsorption capacity of Cu^{2+} on ZSM-5 is calculated by Langmuir model at pH=6 and 45℃ is 86.96 mg/g.

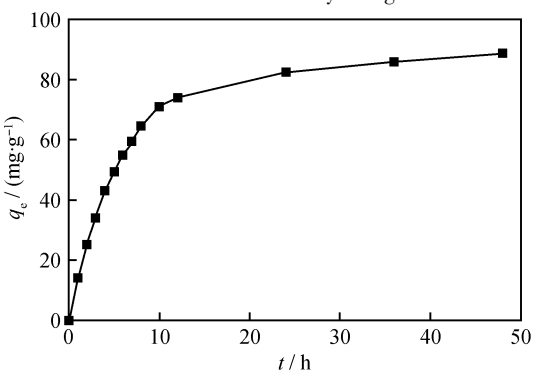

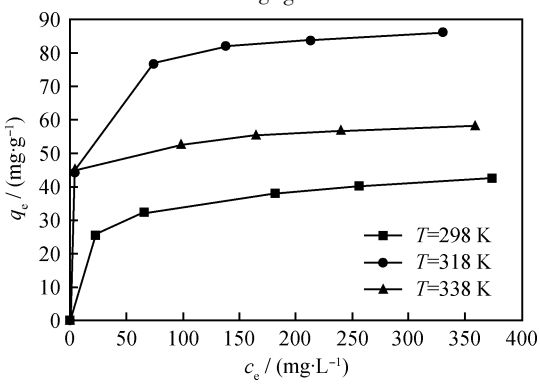

Acta Petrolei Sinica (*Petroleum Processing Section*), 2018, 34(6): 1247-1254 **doi**: 10.3969/j.issn.1001-8719.2018.06.027

Density Functional Theory and Molecular Dynamic Simulation of N_2/CH_4 Separation Over Nanoporous Graphene Membranes

JIA Xiaoxia YANG Jiangfeng WANG Yong LI Jinping

Graphene membrane H-pore-13, with pore size of 0.406 nm, exhibits much higher N_2 separation selectivity from CH_4, with a N_2 permeance of 10^5 GPU (1 GPU=3.35×10^{-10} mol/(s·m^2·Pa)). This suggests that the nanoporous graphene membrane has great potential applications in the upgrading of natural gas.